New Journal of Physics
The open access journal at the forefront of physics
Deutsche Physikalische Gesellschaft DPG | IOP Institute of Physics

# Molecular beam epitaxy of graphene on ultra-smooth nickel: growth mode and substrate interactions

**J M Wofford, M H Oliveira Jr[1], T Schumann, B Jenichen, M Ramsteiner, U Jahn, S Fölsch, J M J Lopes and H Riechert**

Paul-Drude-Institut für Festkörperelektronik, Hausvogteiplatz 5-7, D-10117 Berlin, Germany
E-mail: wofford@pdi-berlin.de and lopes@pdi-berlin.de

Received 10 June 2014, revised 25 August 2014
Accepted for publication 26 August 2014
Published 30 September 2014

*New Journal of Physics* **16** (2014) 093055

doi:10.1088/1367-2630/16/9/093055

## Abstract

Graphene is grown by molecular beam epitaxy using epitaxial Ni films on MgO (111) as substrates. Raman spectroscopy and scanning tunneling microscopy reveal the graphene films to have few crystalline defects. While the layers are ultra-smooth over large areas, we find that Ni surface features lead to local non-uniformly thick graphene inclusions. The influence of the Ni surface structure on the position and morphology of these inclusions strongly suggests that multi-layer graphene on Ni forms at the interface of the first complete layer and metal substrate in a growth-from-below mechanism. The interplay between Ni surface features and graphene growth behavior may facilitate the production of films with spatially resolved multilayer inclusions through engineered substrate surface morphology.

Keywords: graphene, molecular beam epitaxy, graphene–substrate interaction, heteroepitaxy, nickel

[1] Current address: Departamento de Física, ICEx, Universidade Federal de Minas Gerais-UFMG, C.P. 702, 31270-901, Belo Horizonte, MG, Brazil.

## 1. Introduction

The novel physical properties of graphene make it an attractive material for numerous potential applications [1]. Despite this significant scientific and technological potential, difficulties in synthesis continue to limit graphene's industrial adoption.

Recent advances in growing graphene by chemical vapor deposition on Cu substrates have begun to loosen the synthesis bottleneck [2]. The 'wafer-scale', predominantly monolayer thick graphene films yielded by this growth method have drawn significant attention from researchers and technologists. While the electronic properties of these films have yet to match those of exfoliated graphene flakes [3], their quality has been sufficient to allow the demonstration of a number of laboratory devices [4, 5].

However, fully leveraging the potential benefits of graphene will require films which are more than a single monolayer thick [1]. As multiple graphene layers are stacked their electronic properties evolve, with the number of layers and their stacking order determining the specifics [6]. This malleability enables band structure engineering such as opening a band-gap or inducing metallic behavior. Combining in-plane patterning with thickness engineering would allow a further degree of control over the band structure of graphene, facilitating some of the most ambitious graphene-based device architectures. For instance, semiconducting graphene is necessary for transistor channels [7, 8], and metallic graphene might be suitable for device interconnects [9], etc. Although the realization of such devices remains beyond our current capabilities, they do serve to illustrate the advantages of a fully controllable synthesis method which allows for the selective growth of mono-, bi-, and multilayer graphene films.

Reexamining the growth behavior of graphene on Ni substrates as opposed to Cu may allow some of these limitations to be addressed. Ni has previously been demonstrated to support the growth of multilayer graphene films with crystalline quality comparable to growth on Cu [10, 11], and this property has been correlated with the finite solubility of C in the bulk of the metal [12]. However, graphene films grown on Ni tend to be non-uniformly thick, leading to a degradation of the film's overall properties [10]. Transforming the ability of Ni to support the growth of thicker-than-monolayer graphene films from a liability into an asset will require continued progress in understanding the basic science, as well as engineering solutions to the practical obstacles involved.

We report on the growth of graphene on epitaxial Ni films deposited on MgO(111) substrates using molecular beam epitaxy (MBE). MBE has been successfully used in graphene growth on a variety of substrates [13, 14], and this combination of Ni substrate and synthesis method enables a high level of control over the growth process, including over the average thickness of the resulting high-quality graphene films. Graphene growth on Ni is also sensitive to surface contaminants, in particular O [15], which the cleanliness of UHV synthesis helps to mitigate. Both the smoothness of the exclusively (111) oriented Ni surface and the sub-monolayer precision in C deposition we report are improvements over previous, similar growth efforts [16]. Furthermore, the overall film quality resulting from MBE allows the examination of graphene growth behaviors which might otherwise have been obscured. For instance, we find that step clusters and other Ni surface features significantly influence graphene growth. These observations suggest that any subsequent graphene after the first complete monolayer forms at the interface of the existing film and the Ni substrate. Graphene growth by MBE thus offers not only high-quality films, but also insight into the fundamental processes which underpin the synthesis of this remarkable material.

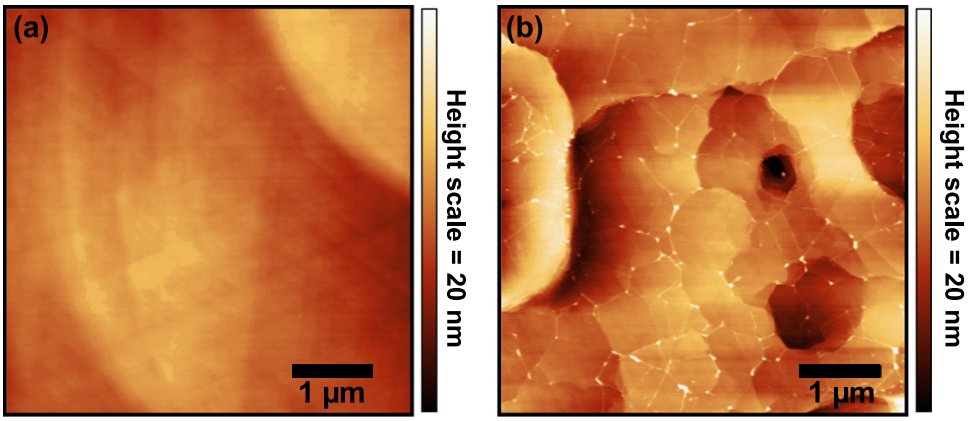


**Figure 1.** Atomic force microscopy images of a 150 nm thick, epitaxial Ni film on MgO (111) (a), and a similar Ni film covered in graphene (b) (200 min deposition time). Notice the exceptionally smooth surface of the Ni in (a), and that this surface quality persists after C deposition (b). The cellular network of wrinkles in the graphene film caused by the thermal contraction of the substrate is also visible in (b).

## 2. Experimental methods

All samples were grown in an MBE reactor with a base pressure of $2.5 \times 10^{-10}$ torr. The substrates used were commercially purchased MgO(111) (CrysTec GmbH, single-side polished, $1 \times 1$ cm, 1 $\mu$m Ti back coating). The 150 nm thick Ni films were prepared following the recipe of Iwasaki *et al* with MBE substituted for dc sputtering [17]. First a 50 nm thick 'buffer layer' of Ni is deposited at 300 °C, then the substrate temperature is raised to 600 °C and the remaining 100 nm of Ni is deposited. The Ni was evaporated from a standard high-temperature effusion cell, and the epitaxial relationship between the two materials was confirmed by both reflection high energy electron diffraction and x-ray diffraction. The films were smoothed by heating them to 850 °C for 20 min, resulting in a Ni surface which is extremely flat over tens of microns (figure 1(a)). Carbon was then deposited on the Ni–MgO(111) from a resistively heated, pyrolytic graphite filament (MBE Komponenten GmbH, SUKO-type cell). All graphene growths were performed at a substrate temperature of 765 °C, with deposition times varying from 40 to 200 min. Samples were cooled at a rate of 25 °C $\text{min}^{-1}$ to 350 °C, and then $\sim$10 °C $\text{min}^{-1}$ until the ambient was reached. Scanning electron microscopy (SEM) and Raman spectroscopy indicate that this range of deposition times yields 0.7–3.5 monolayers of graphene. Ni films prepared following this procedure but excluding deliberate C deposition showed no evidence of graphene formation. The resulting graphene films were also examined using atomic force microscopy (AFM) and scanning tunneling microscopy (STM).

## 3. Results and discussion

We first examined the graphene–Ni using AFM to determine whether the surface quality of the epitaxial Ni films was preserved throughout the C deposition process. Even as the Ni morphology continues to evolve during C deposition, its overall smoothness remains exceptional (figure 1(b)). As noted by Iwasaki *et al* holding a Ni film at high-temperature for an extended period led to the formation of 'pits' in the metal, but this could be avoided by

monitoring the thermal budget of the sample [17]. Also visible in figure 1(b) is the characteristic cellular structure formed by wrinkles in the graphene film. These localized areas of graphene–substrate delamination form to alleviate mechanical stress which develops from the greater substrate contraction during sample cooling.

When evaluating the graphene itself it is helpful to first consider the interplay between the various C–Ni bulk and surface phases present during growth. Among these phases are the gas of C adatoms on the Ni surface, the solid solution of C in bulk Ni, the $Ni_2C$ surface carbide, and the graphene itself. The $Ni_2C$ surface phase is unstable at the growth temperature used here and is unlikely to contribute to these results [18]. It is also important to distinguish between mono- and multilayer graphene on Ni(111) due to the free-energy reduction caused by hybridization and charge transfer between the Ni *d*-bands and the $\pi$-bands of the graphene in direct contact with it. Evidence of this bonding can be seen in the changes to the monolayer graphene band structure [19, 20] and phonon dispersion [21] which effectively quench its Raman signal, and in its higher thermal stability with respect to dissolution into the Ni metal. For example, only monolayer graphene is stable on the (111) surface of bulk Ni (with a 'very low C concentration') at 605 °C, but it too dissolves into the metal when the temperature is raised to 655 °C [22, 23]. When there is a preexisting concentration of C in the Ni substrate the driving force for dissolution can be negated; if equilibrium is reached no net dissolution occurs, and the graphene is stable at significantly higher temperatures [24]. Thus, the 765 °C growth temperature used here likely led the C concentration within the Ni film to increase prior to the nucleation and growth of mono- or multilayer graphene.

The 'quality', or crystalline perfection, of the graphene was initially evaluated by Raman spectroscopy. Spectra were collected from individual features in the graphene films using a 1 $\mu$m laser spot size, allowing the observation of local film properties. The quenching of the Raman signal by the monolayer graphene–Ni bonding is not an obstacle to this analysis because it does not persist beyond the first graphene layer. For instance, a Raman examination of a graphene film deposited for 80 min did not indicate a continuous graphene film across the entire Ni surface, while SEM imaging showed there to be no exposed Ni between bilayer portions of the film (which were easily observed by Raman, see figure 2). The Raman spectra presented here are thus from bilayer or thicker regions of graphene, where the layer(s) not in direct contact with the Ni surface remain detectable.

A representative Raman spectrum from the same 80 min graphene film is shown in figure 2. This particular spectrum is that of monolayer graphene, suggesting this region of the film is in fact bilayer graphene (with the 'bottom', Ni-bound graphene isolating the 'top' layer, but not contributing directly). Figure 2 also exhibits a symmetric 2D peak showing that the two graphene sub-lattices within the top layer remain equivalent, possibly as the result of a lattice rotation. The intensity of the D peak is substantially lower than the G and 2D peaks, which is commonly accepted as an indication of a low defect concentration. The G and 2D peaks have narrow FWHM values (29 $cm^{-1}$ and 41 $cm^{-1}$, respectively), further indicating a high degree of crystalline order. Overall, Raman spectra from graphene films grown on Ni–MgO(111) substrates by MBE indicate they contain very few crystalline defects.

The quality of the graphene films was confirmed through direct observation using STM. The 200 min deposition time of this film resulted in ~3.5 monolayers of graphene, one of the thickest films grown here. Figure 3(a) shows that the hexagonal, $sp^2$ C lattice is atomically perfect over the area examined, with no point- (vacancies, Stone–Wales) or line-defects (rotational boundaries) present. The individual hexagons of C atoms are easily visible in the

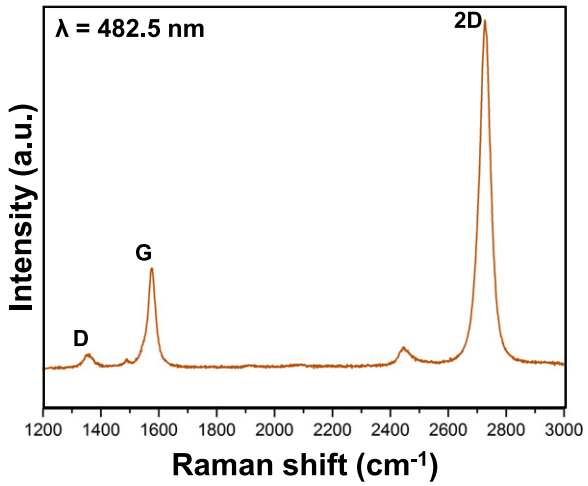


**Figure 2.** Raman spectrum from graphene grown on Ni–MgO(111) (80 min deposition time). The narrow FWHM of the G and 2D peaks, and the low intensity of the D peak, are indicative of high quality graphene.

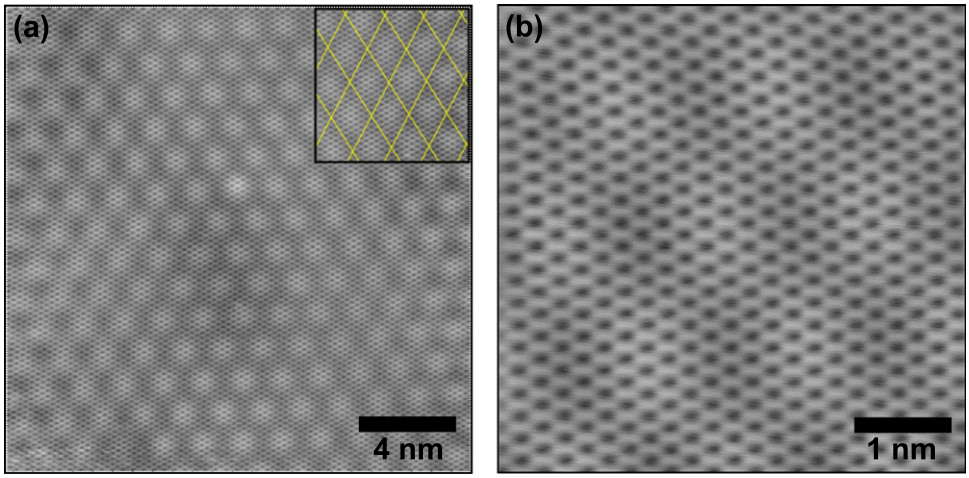


**Figure 3.** Constant-current STM images (0.1 nA, 0.1 V) of graphene grown on Ni–MgO (111) (200 min deposition time). The graphene lattice is atomically perfect over the region investigated (a), with the individual hexagons of C atoms easily visible in the high-resolution scan (b). Also visible is the moiré pattern caused by the superposition of two graphene lattices rotated relative to each other (see boxed overlay in (a)).

higher resolution STM image in figure 3(b). Also discernable is the moiré pattern formed by the superposition of the two graphene lattices. The orientation and periodicity (17 Å) of the moiré are consistent with the two graphene layers being rotated by 8.3° relative to one another [25].

We next consider the process by which thickness inhomogeneities develop in graphene films during growth on Ni. Such thickness inclusions are typical of most graphene films synthesized on Ni [10, 11, 26, 27]. Here, we examine this phenomenon using Raman spectroscopy and SEM. The thicker regions of the graphene film do not develop prior to the formation of a continuous monolayer of graphene across the entire Ni surface. Evidence of this is offered by the absence of multilayer regions of graphene in samples with ∼1 monolayer or less of graphene (figure 4). This is also consistent with monolayer graphene bound to Ni(111)

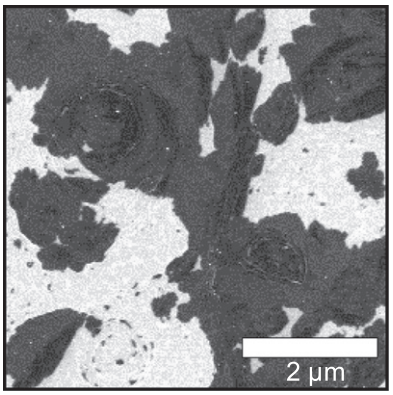


**Figure 4.** In-lens detector SEM image of a sub-monolayer graphene film on Ni–MgO (111) (40 min deposition time). The dark regions are graphene, while the lighter areas are bare Ni. The constant contrast within the regions covered by graphene indicates they are exclusively monolayer.

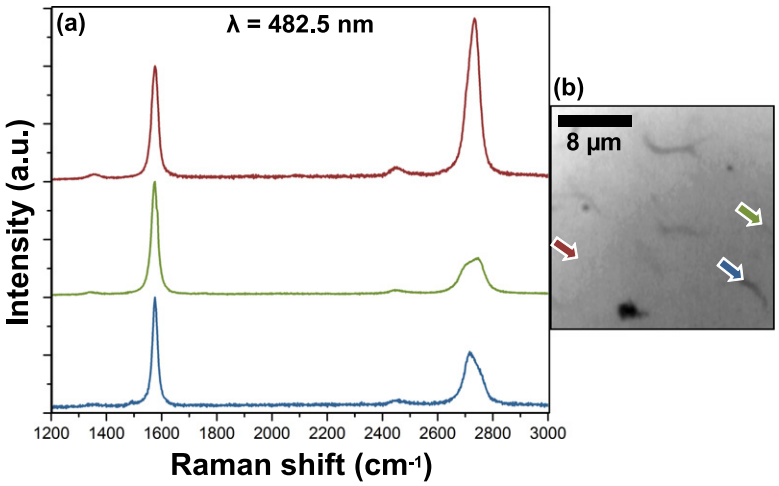


**Figure 5.** Raman spectra (a) from a graphene film grown on Ni–MgO(111), and an optical micrograph (b) indicating the physical location each was collected (200 min deposition time, the longest used here). The spectra are characteristic of bi- (green) and likely trilayer (blue) bernally stacked graphene, as well as turbostratic multilayer regions (brown). The illumination in (b) is somewhat uneven, enhancing the contrast for the blue location. Because the first graphene layer does not contribute, this is consistent with a 3–4 monolayer thick graphene film. The graphene stacking at each location was extracted from the shape of the 2D peak (at ~2700 $cm^{-1}$) [28], the spectra were scaled to the height of the G peak, and offset for visibility.

being the thermodynamically preferred phase, with the less favorable multilayer state not being occupied until the first monolayer is complete.

Figure 5 illustrates the variability that develops in thicker graphene films (200 min deposition time). The spectra indicate the majority of this film is three- and four-layer graphene, since they are characteristic of AB-stacked bi- and trilayer graphene (figure 5 green, blue). A minority of spectra from this film have a symmetric 2D peak (figure 5, brown), confirming that rotational disorder sometimes occurs between graphene layers (as observed by STM) [28]. It

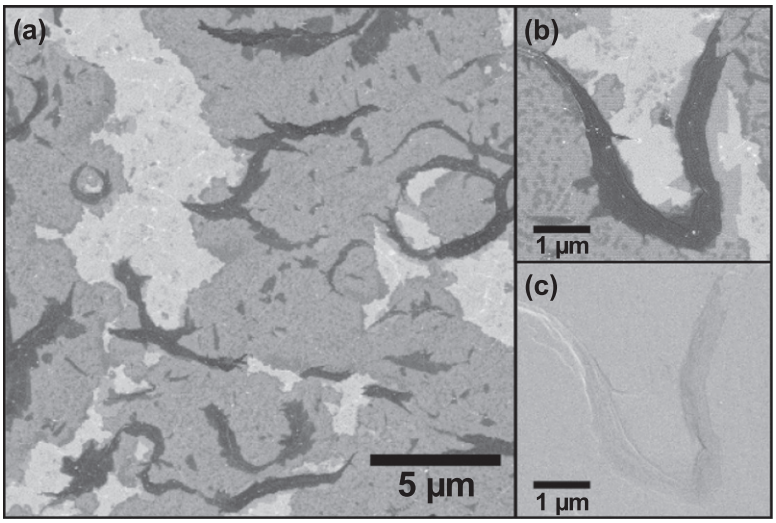


**Figure 6.** SEM images of graphene grown on Ni–MgO(111) collected with in-lens (a, b) and Everhart–Thornley detectors (c) (200 min deposition time). Darker contrast in (a), (b) corresponds to thicker graphene. Multilayer regions of graphene tend to grow on top of step edge clusters on the Ni substrate, leading them to form into extended ribbons (a). Imaging the same region using different SEM detectors clearly illuminates the correlation between thicker graphene (b) and surface steps (c).

has been shown that such rotational disorder is more common in graphene grown on Ni above ~650 °C [29]. Possible methods to minimize this effect through the sample cooling rate etc were not systematically examined here.

Mapping the spatial distribution of the thickness inhomogeneities using SEM offers further insight into their origin. By simultaneously imaging the graphene films with two different detectors, it is possible to correlate the thickness variations with the morphology of the underlying Ni surface. Immediately noticeable in the large field-of-view SEM image in figure 6(a) is that, rather than forming compact or dendritic islands, the thicker regions of the graphene film instead form extended ribbons. When SEM micrographs collected simultaneously with the in-lens detector (figure 6(b))—which is more sensitive to the atomic number—and the Everhart–Thornley detector (figure 6(c))—which shows the surface topology—are compared it becomes apparent the ribbons of thicker graphene coincide with step-clusters on the surface of the Ni substrate. The elongated ribbons formed by the thicker regions of the graphene film reflect the extended nature of the step clusters, and this is consistent with the distribution of thicker regions in figure 6(a).

SEM also reveals the precise morphology of the thicker regions within the graphene film. Of particular interest are the jagged perimeters of many of these regions, which are composed of straight sections joined at 60° or 120° angles (figure 7, also visible in figure 6(b)). This type of boundary shape is unlikely to be the result of edge-energy-minimization, as computational [30] and experimental [22] studies concur that strongly faceted island shapes are not preferred on Ni. The jagged, or 'saw tooth' graphene edges may instead result from the particular morphology of the Ni surface on which they grew. For instance, graphene sheets terminated at steps in the Ni (111) surface which are parallel to its in-plane, close-packed [1–10] directions would produce such shapes.

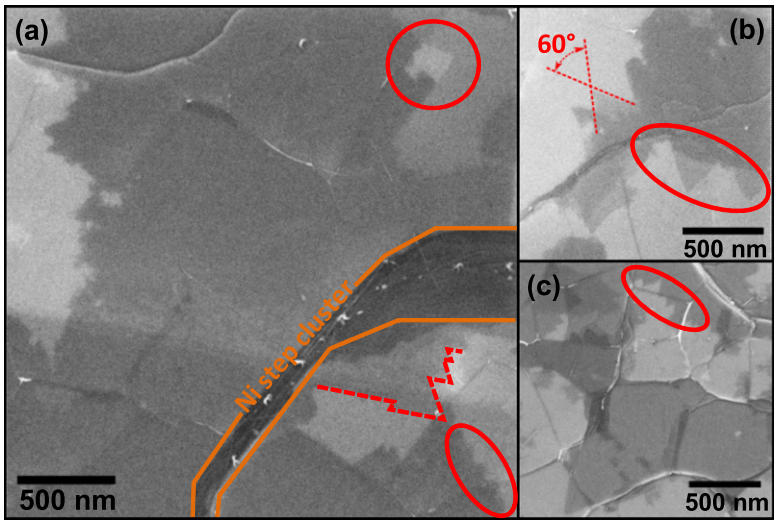


**Figure 7.** In-lens detector SEM images of graphene grown on Ni–MgO(111) (120 min deposition time). Darker contrast corresponds to thicker graphene. In addition to often being situated on Ni step clusters (a), thicker regions of graphene sometimes have jagged perimeters composed of straight sections and 60° or 120° angles (b). A particularly illustrative example is shown by the red dashed line in (a), while the red ovals in (b) and (c) highlight selected other instances.

The interpretation that the saw-tooth perimeters of the thicker graphene regions result from the structure of the Ni surface is supported by a meticulous AFM examination. Specifically, comparing AFM height and phase information shows how individual Ni surface steps may influence graphene growth. Figure 8 displays a pair of such images from a film with a 200 min deposition time. The entire sample surface is covered by the inhomogeneously thick graphene film. The height scan (figure 8(a)) contains the expected features: graphene wrinkles, steps within the graphene film marking the edges of monolayers (and thus transitions to thicker or thinner portions of the continuous graphene film, green arrow in figures 8(a) and (c)), and Ni substrate steps. Two distinct regions are identifiable in the phase information (figure 8(b)), differentiated by the presence of a periodic superstructure. Its periodicity and hexagonal symmetry suggest the superstructure is a moiré formed by graphene layers of different crystallographic orientation (similar to figure 3). This means the perimeter of the super-structured region is unambiguously the edge of an incomplete graphene layer.

It is significant that the transition from the superstructure to 'smooth' graphene coincides with easily observable, $0.5 \pm 0.05$ nm steps in the height image (see blue arrow in figures 8(a) and (c)). This step height is consistent with a combination of one Ni atomic step (0.2 nm) and one graphene step (0.33 nm, between layers in a multilayer film such as this one). That the graphene monolayer terminates directly at a Ni step shows that a graphene growth front may be impeded by step edges in the Ni surface. This implies the jagged perimeters of the thicker portions of the graphene film are caused by the step distribution and structure of the underlying Ni. More generally, it further illustrates how the Ni surface morphology can directly influence graphene growth; in addition to thicker graphene inclusions being situated on Ni *step clusters*, it is also possible for *individual* Ni steps to alter the propagation of a graphene monolayer.

The interactions between the thicker regions of the graphene film and the Ni surface allow details regarding the kinetics of the growth process to be inferred. The localization of thicker

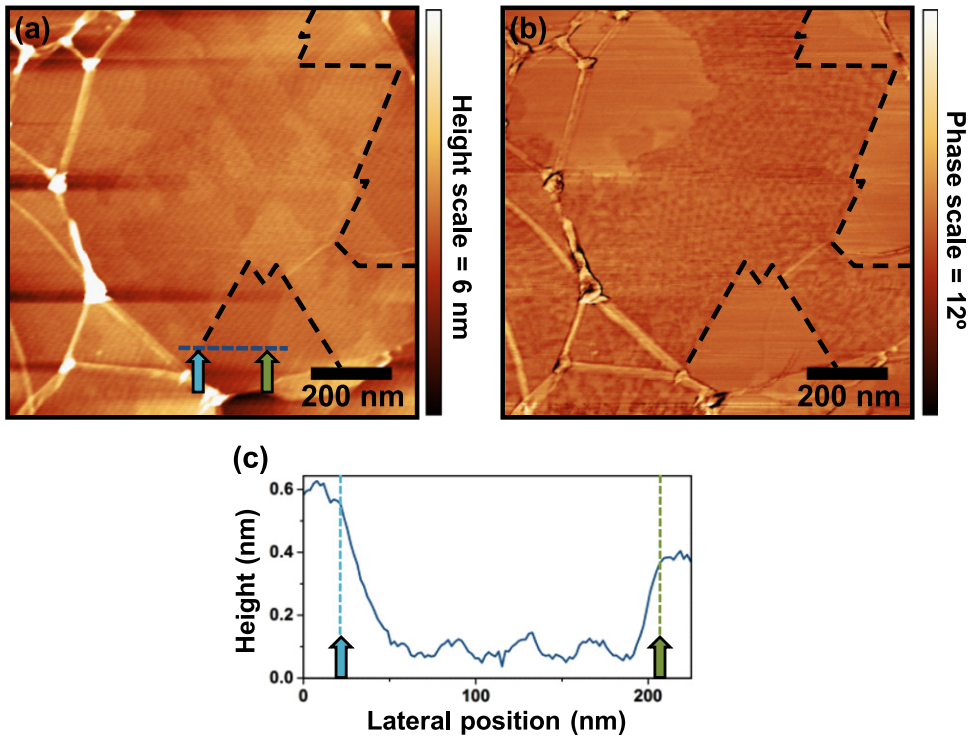


**Figure 8.** AFM height (a) and phase (b) scans of graphene grown on Ni–MgO(111) (200 min deposition time). The profile in (c) is from the dashed blue line in (a), and the green arrows in (a) and (c) mark the edge of a graphene sheet (~0.33 nm step) while the blue arrows mark a combination Ni–graphene step (~0.53 nm step, measured heights are ±0.05 nm). The black outlines in (a) and (b) mark the perimeter of regions in the graphene film which display no superstructure (and thus the edge of a partial graphene monolayer). The transition from the superstructure to 'smooth' graphene coincides with a combined graphene–Ni step.

graphene inclusions at Ni step clusters, as well as the role sometimes played by individual Ni steps in determining their lateral expansion, indicates the graphene layer in question is in direct contact with the Ni surface. Because a continuous monolayer film of graphene forms prior to any multilayer regions, the additional graphene layers must grow at the interface between that first graphene monolayer and the Ni substrate (see figure 9 for a schematic illustrating this process). The further graphene layers do not grow on top of the previously deposited C film. Graphene on Ni–MgO(111) substrates is thus likely an additional instance of 'growth from below'.

A possible cause of the additional growth at the graphene–Ni interface is thermally driven C precipitation from the Ni substrate during sample cooling. Indeed, when precipitation from the C–Ni solid solution is the only source of C during graphene growth on Ni, exactly this scenario occurs [31]. While growth from thermally driven precipitation likely also occurs here, it is insufficient to fully explain the behavior observed. First and foremost, the amount of thicker graphene—both in total area and thickness—scales with the deposition time. Similarly, a 150 nm thick Ni film fully saturated at 765 °C would not contain sufficient C to account for the observed thicker regions of graphene at longer deposition times [32]. Thus the thicker ribbons of graphene must develop during C deposition.

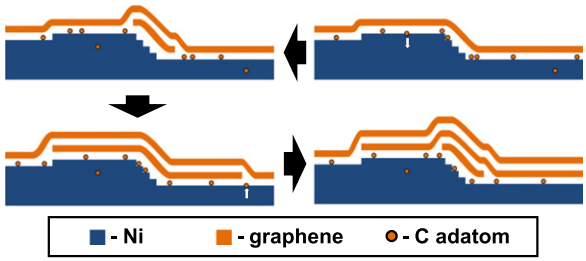


**Figure 9.** A schematic showing how graphene 'grows from below' on Ni(111). Rather than nucleating on the exposed surface of the first complete layer, subsequent graphene layers instead nucleate and grow directly on the Ni surface below the existing layer. It is possible the additional graphene layers nucleate heterogeneously at step edge clusters in the Ni surface. The expansion of graphene monolayers can also be interrupted by individual steps in the Ni surface (see second monolayer growing to the left in the schematic above).

The growth from below mechanism has most recently been examined during graphene growth on metal substrates with both finite and negligible C solubilities. A combined low-energy electron microscopy and diffraction (LEED) study of graphene growth on Ir(111) reveals that the nucleation and growth of the second graphene layer occurs at the interface between the first complete layer and the metal substrate [33]. A similar, if forensic, analysis of graphene grown on the (001) oriented grains of Cu foils reached a similar conclusion. By comparing the relative LEED intensities from the upper and lower graphene layers of a partially bilayer film it was shown that the smaller, lower graphene sections are between the larger graphene crystals and metal substrate [34]. The apparent ubiquity of growth from below on metals, Ni included, is perhaps less surprising when the variety of species with which graphene has been successfully intercalated is considered [20, 35, 36].

Although several important differences complicate direct comparisons, it is useful to further examine these results in the context of previous studies of graphene growth on Ni. Unlike many examples in the literature, where bulk Ni or thicker films were used as substrates, the Ni films used here are thin enough to ensure graphene formation prior to sample cooling even at temperatures above its stability on the pure metal. The nucleation and growth behavior observed is thus that of graphene in approximate equilibrium with the opposing dissolution process. This could be particularly significant, for instance, during graphene nucleation. The competition between graphene formation and C absorption into the substrate has been observed to enhance concentration gradients in the surface gas of C adatoms during growth on Ni [22]. Both the evolution of existing graphene islands and any subsequent nucleation events will be influenced by this uneven C concentration. The localization of multilayer graphene inclusions at step edge clusters observed here may be assisted by the absence of such concentration gradients.

It is interesting to consider if graphene growth on Ni saturated with C is a bulk or surface mediated process; or, whether surface or bulk diffusion dominates mass transfer to the graphene growth front. Potentially relevant experiments such as the isotope labeling work of the Ruoff group offer little insight because thermal precipitation from the well-mixed solid solution would mask any related details, leaving us to examine less directly related work [12]. In the regime defined by a growth temperatures below the thermal stability of monolayer graphene on pure Ni combined with an unsaturated Ni substrate, it has been shown to be a surface mediated process [22]. These experiments also show that the free C on the Ni surface leads to a change in electron

reflectivity, which is evidence of a high adatom gas concentration during graphene growth on Ir (111) and Ru(0001) [37, 38]. Also, it is the supersaturation of the surface gas by the external C flux which must be responsible for initiating graphene nucleation, as the surface gas will mediate any interaction between the solid solution and nascent graphene during nucleation. Combined with the higher rate of diffusion on surfaces, these considerations tend to support a surface dominated process. However, sufficient exchange between the solid solution and surface gas could lead bulk diffusion to dominate, leaving this an open question. Regardless of whether intercalative surface diffusion or bulk diffusion and precipitation dominates, it is fascinating that this state remains kinetically accessible to C adatoms even as the substrate is covered by a progressively thicker continuous graphene film. This ongoing accessibility is a fundamental difference between graphene growth on Ni and, for instance, Cu, where even continued deposition of elemental C does not lead to multilayer formation [39].

In addition to offering evidence of the growth-from-below mechanism, graphene–substrate interactions during growth on Ni may provide an added tool with which to influence film structure. It is interesting that as they develop between the existing graphene film and the Ni substrate the thicker regions of graphene do so at step edge clusters in the Ni surface. That substrate step clusters have been shown to act as heterogeneous nucleation sites during graphene growth on other metal surfaces makes it a reasonable interpretation of the behavior observed here [39, 40]. This points to the intriguing possibility of using Ni substrates with engineered stepped surfaces to guide the nucleation and growth of multilayer inclusions in a graphene film. Alternatively, exclusively monolayer films may be facilitated by using highly stepped regions of the substrate (such as deliberate pits in the metal) to getter excess carbon. Although the 765 °C growth temperature used here led to continued surface evolution during growth, a lower growth temperature would significantly increase the stability of an engineered Ni surface. Any growth temperature above the ∼600 °C thermal stability of monolayer graphene on pure Ni would result in similar growth behavior. The intrinsic properties of the graphene–Ni growth system make it a possibility to produce the spatially engineered multilayer graphene films which are ideal for future applications.

## 4. Conclusion

We have demonstrated the utility of MBE for synthesizing graphene heterostructure by growing high-quality films using epitaxial Ni on MgO(111) as substrates. In addition to providing a template for low-defect growth, the exceptionally smooth MBE grown Ni surface has allowed the identification of a number of growth behaviors which might otherwise have been obscured. We find that the C films have the thickness inhomogeneities typical of graphene grown on Ni, but that the thicker regions are closely correlated with step edge clusters on the substrate surface. Furthermore, SEM and AFM show that the thicker graphene regions often have jagged perimeters, which result from the Ni surface morphology. Taken together these observations suggest the growth of multilayer graphene on Ni occurs at the interface of the existing graphene film and the metal, rather than on the exposed top surface of the graphene. Combined with an engineered Ni surface, this growth mode may allow the distribution of the thickness inhomogeneities to be influenced. Such a scheme would facilitate the production of graphene films with spatially resolved bi-, tri-, and multilayer inclusions, which are ideal for future applications.

## Acknowledgements

The authors would like to thank Claudia Herrmann, Michael Höricke, and Hans-Peter Schönherr for their valuable support of the research presented here, and Dr Jos Boschker for his helpful comments on the manuscript. JMW acknowledges support from a Leibniz Association Postdoctoral Fellowship and an Alexander von Humboldt Postdoctoral Research Fellowship.

## References

[1] Novoselov K S, Fal'ko V I, Colombo L, Gellert P R, Schwab M G and Kim K 2012 *Nature* **490** 192–200
[2] Li X *et al* 2009 *Science* **324** 1312
[3] Cao H *et al* 2010 *Appl. Phys. Lett.* **96** 122106
[4] Lee S, Lee K, Liu C-H, Kulkarni G S and Zhong Z 2012 *Nat. Commun.* **3** 1018
[5] Wu Y, Lin Y, Bol A A, Jenkins K A, Xia F, Farmer D B, Zhu Y and Avouris P 2011 *Nature* **472** 74
[6] Castro Neto A H, Peres N M R, Novoselov K S and Geim A K 2009 *Rev. Mod. Phys.* **81** 109
[7] Oostinga J B, Heersche H B, Liu X, Morpurgo A F and Vandersypen L M K 2008 *Nat. Mater.* **7** 151
[8] Zhang Y, Tang T-T, Girit C, Hao Z, Martin M C, Zettl A, Crommie M F, Shen Y R and Wang F 2009 *Nature* **459** 820
[9] Hertel S, Waldmann D, Jobst J, Albert A, Albrecht M, Reshanov S, Schöner A, Krieger M and Weber H B 2012 *Nat. Commun.* **3** 957
[10] Reina A, Jia X, Ho J, Nezich D, Son H, Bulovic V, Dresselhaus M S and Kong J 2009 *Nano Lett.* **9** 30
[11] Kim K S, Zhao Y, Jang H, Lee S Y, Kim J M, Kim K S, Ahn J, Kim P, Choi J and Hong B H 2009 *Nature* **457** 706
[12] Li X, Cai W, Colombo L and Ruoff R S 2009 *Nano Lett.* **9** 4268
[13] Moreau E, Godey S, Ferrer F J, Vignaud D, Wallart X, Avila J, Asensio M C, Bournel F and Gallet J-J 2010 *Appl. Phys. Lett.* **97** 241907
[14] Lippert G, Dabrowski J, Yamamoto Y, Herziger F, Maultzsch J, Baringhaus J, Tegenkamp C, Lemme M C, Mehr W and Lupina G 2012 *Phys. Status Solidi* **249** 2507
[15] Grandthyll S, Gsell S, Weinl M, Schreck M, Hüfner S and Müller F 2012 *J. Phys.: Condens. Matter* **24** 314204
[16] Garcia J M *et al* 2010 *Solid State Commun.* **150** 809
[17] Iwasaki T, Park H J, Konuma M, Lee D S, Smet J H and Starke U 2011 *Nano Lett.* **11** 79
[18] Lahiri J, Miller T S, Ross A J, Adamska L, Oleynik I I and Batzill M 2011 *New J. Phys.* **13** 025001
[19] Shikin A, Prudnikova G, Adamchuk V, Moresco F and Rieder K-H 2000 *Phys. Rev.* B **62** 13202
[20] Varykhalov A, Sánchez-Barriga J, Shikin A M, Biswas C, Vescovo E, Rybkin A, Marchenko D and Rader O 2008 *Phys. Rev. Lett.* **101** 157601
[21] Allard A and Wirtz L 2010 *Nano Lett.* **10** 4335
[22] Addou R, Dahal A, Sutter P and Batzill M 2012 *Appl. Phys. Lett.* **100** 021601
[23] Dahal A and Batzill M 2014 *Nanoscale* **6** 2548
[24] Shelton J C, Patil H R and Blakely J M 1974 *Surf. Sci.* **43** 493
[25] Miller D L, Kubista K D, Rutter G M, Ruan M, de Heer W A, First P N and Stroscio J A 2010 *Phys. Rev.* B **81** 125427
[26] Obraztsov A N, Obraztsova E A, Tyurnina A V and Zolotukhin A A 2007 *Carbon* **45** 2017
[27] Yu Q K, Lian J, Siriponglert S, Li H, Chen Y P and Pei S S 2008 *Appl. Phys. Lett.* **93** 113103
[28] Malard L M, Pimenta M A, Dresselhaus G and Dresselhaus M S 2009 *Phys. Rep.* **473** 51
[29] Dahal A, Addou R, Sutter P and Batzill M 2012 *Appl. Phys. Lett.* **100** 241602
[30] Artyukhov V I, Liu Y and Yakobson B I 2012 *Proc. Natl Acad. Sci. USA* **109** 15136
[31] Odahara G, Otani S, Oshima C, Suzuki M, Yasue T and Koshikawa T 2011 *Surf. Sci.* **605** 1095

[32] Lander J J, Kern H E and Beach A L 1952 *J. Appl. Phys.* **23** 1305
[33] Nie S, Walter A L, Bartelt N C, Starodub E, Bostwick A, Rotenberg E and McCarty K F 2011 *ACS Nano* **5** 2298
[34] Nie S, Wu W, Xing S, Yu Q, Bao J, Pei S and McCarty K F 2012 *New J. Phys.* **14** 093028
[35] Grüneis A and Vyalikh D 2008 *Phys. Rev.* B **77** 193401
[36] Shikin A M, Adamchuk V K and Rieder K-H 2009 *Phys. Solid State* **51** 2390
[37] Loginova E, Bartelt N C, Feibelman P J and McCarty K F 2008 *New J. Phys.* **10** 93026
[38] Loginova E, Bartelt N C, Feibelman P J and McCarty K F 2009 *New J. Phys.* **11** 063046
[39] Wofford J M, Nie S, McCarty K F, Bartelt N C and Dubon O D 2010 *Nano Lett.* **10** 4890
[40] Wofford J M, Starodub E, Walter A L, Nie S, Bostwick A, Bartelt N C, Thürmer K, Rotenberg E, McCarty K F and Dubon O D 2012 *New J. Phys.* **14** 053008